ChemComm

Accepted Manuscript

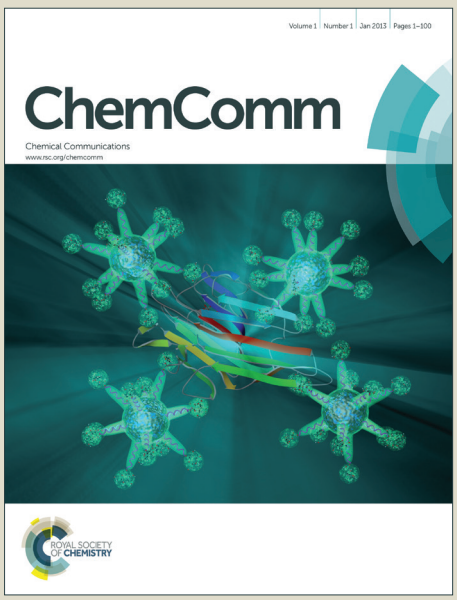

ROYAL SOCIETY OF CHEMISTRY

www.rsc.org/chemcomm

ChemComm RSCPublishing

COMMUNICATION

Progressive Acylation of Pyrene Engineers Solid State Packing and Colour via C-H···H-C, C-H···O and π-π Interactions†

Cite this: DOI: 10.1039/x0xx00000x

Received 00th January 2014,
Accepted 00th January 2014

DOI: 10.1039/x0xx00000x

www.rsc.org/

Shinaj K. Rajagopal, Abbey M. Philip, Kalaivanan Nagarajan and Mahesh Hariharan*

Quantum theory of atoms in molecules and Hirshfeld surface analyses indicated increase in the extent of i) C–H···H–C; ii) C–H···O, iii) π–π interactions and decrease in the extent of i) σ–π interaction, ii) interplanar angle between the vicinal pyrene units in a series of acetylpyrene derivatives offering blue-green-orange emissive crystals.

Molecular crystal engineering[1] of polyaromatic hydrocarbons to yield 1–2D lamellar arrangement demonstrated pivotal role in photonic[2] and semiconductor device applications.[3] Extended orbital overlap through π–columnar stacks compared to herringbone arrangement of arenes is proven to be vital.[4] Recent efforts in transforming herringbone to columnar arrangement of arenes through various methods such as chemical modifications,[5] co-[6] and solvent-crystallization,[7] heat-mode,[8] mechanical stimulation[9] and solid seeding[10] validate to be effective. Achieving diverse degree of orbital overlap between the neighboring units in the crystalline state is still a challenging task. Monitoring the effect of subtle orientation differences and thereby the orbital overlap between the neighboring units in arenes is even more challenging. Extent of orbital overlap through π–π interactions between the vicinal arenes could be reflected in the optical properties of the crystals.[11] Extremely high sensitivity of pyrene fluorescence towards environmental effects can amplify the consequence of orientation factor/orbital overlap between the adjacent units.[12]

Our ongoing interest to regulate the arene-arene interactions in fluorescent crystals,[13] vesicular gels[14] and thin films prompted us to explore the correlation between optical properties *vs.* peripheral substitution of pyrene. We employ simple and convenient Friedel–Crafts reaction, invented 137 years ago,[15] to increase the number of carbonyl groups in pyrene. Carbonyl conjugated arenes in solution exhibit diverse excited state processes[16] depending on adjacent functionality such as i) low fluorescent (Φ_f < 0.002) aryl aldehydes/ketones dominated by intersystem crossing (ISC); ii) moderate fluorescent secondary/tertiary carboxamides[17] dominated by internal conversion and iii) high fluorescent aryl acids/esters[18] dominated by radiative process. Extremely low Φ_f in solution hampered the efforts to explore the optical properties of aryl ketones/aldehydes in the crystalline state though plethora of pyrene derivatives is explored for optoelectronic applications.[19]

Furthermore, heteropolar C–H···H–C interactions are rarely found as an integral force in organic crystals when compared to C–H···O,[20] C–H···π,[21] homopolar C–H···H–C[22] interactions etc. Heteropolar C–H···H–C interactions could arise from dipolar/quadrupolar nature of sp^2 C–H bond that could induce dipole on the vicinal sp^3 C–H unit. Highly electronegative substituents/groups adjacent, either geminal or vicinal, to sp^2 C–H unit may polarize the bond allowing extended interactions.[23] We herein report for the first time a systematic control on the organization of adjacent pyrene units through the progressive addition of acetyl groups that transforms sandwich herringbone structure of pyrene to columnar arrangement in tri/tetraacetylpyrene. Distinct packing arrangement, through C–H···H–C, C–H···O and π–π interactions, in acetylpyrene derivatives offer diverse solid-state colouring and fluorescent properties.

Adding stoichiometric quantity of acetyl chloride to a solution of pyrene and $AlCl_3$ in carbon disulfide (CS_2) at ambient temperature rendered the desired acetyl derivatives (**1**–**4AP**) with moderate yields (Scheme 1, Row I).[24] Compounds (**1**, **2**, **2'**, **2"**, **3AP**) were crystallized by varying acetone:hexane composition, whereas **4AP** was obtained by temperature gradient cooling in chloroform. Acetyl derivatives (**1**, **2**', **2"**, **3**, **4AP**) yield solvent free monoclinic crystal system except for **2AP** that exhibits solvent free orthorhombic crystal system (Scheme 1, Row II; Table S1, Electronic Supplementary Information (ESI†)). Differential scanning calorimetric (DSC) analysis of 1-acetylpyrene (**1AP**) exhibited a sharp melting transition (T_m) at 90.4°C (Fig. S1a, ESI†). A significant decrease (ca. 63°C) in the T_m of **1AP** when compared to the T_m of model compound pyrene (**P**)[25] is indicative of attenuation in the ordered arrangement of the crystalline **1AP**. However, further increase in the number of acetyl groups in the pyrene core resulted in a near-linear increase (Fig. S1b, ESI†) in the T_m having a maximum of 295.6°C as in symmetric **4AP** derivative. Similar trend was observed for the change in enthalpy during melting process for **1**–**4AP** (Fig. S1c and Table S2, ESI†).

Qualitative analyses of the single crystal X-ray structure of **1**–**4AP** indicate intra- and intermolecular distances between methyl and

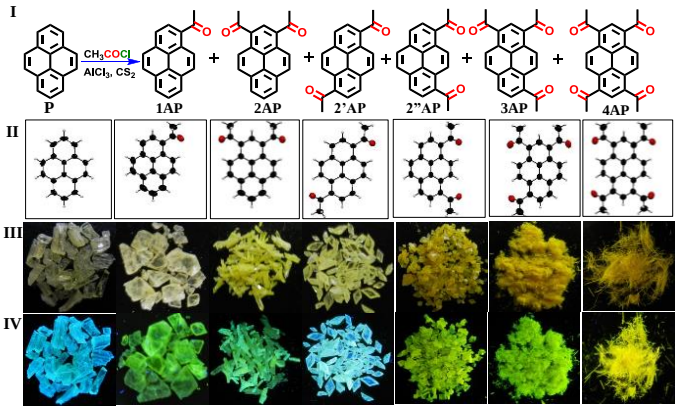

Scheme 1 Row I: Molecular structure of **1**–**4AP**; Row II: corresponding single crystal X-ray structure. Photographic image of the crystals Row III: in daylight; and Row IV: under UV illumination. X-ray structure of **P** is taken from the literature.[26]

aryl hydrogens in the range of 2.098–2.4 Å (Table S3-S4, ESI†). Distances appearing at less than the double of van der Waal's radius of hydrogen atom (2.4 Å) could indicate the existence of dihydrogen (H···H) bonding.[27] Quantum theory of atoms in molecules analyses[28] (QTAIM) of the crystalline **1**–**4AP** offered no characteristics supporting the intramolecular dihydrogen interactions at distances less than 2.4 Å. Intermolecular C–H···H–C interactions in crystalline **2**, **3** and **4AP** (Fig. S2, ESI†) are exemplified through the values of electron density at the (3,–1) bond critical point (BCP; $\rho_b(r)$), its Laplacian ($\nabla^2\rho_b(r)$), the interaction distance (*d*) as indicated in Table 1 (also see Table S4, ESI†), a bond and virial path in the potential energy density map. A closed-shell intermolecular C–H···H–C interaction possessing considerable bond path between a pair of similar hydrogens (CH_3) is seen in **2AP** (Fig. S2a, ESI†). Non polar C–H···H–C interaction evaluated accumulation of electron density, $\rho_b(\mathbf{r})$, 0.036 eÅ^{-3} and the positive value of the Laplacian at the BCP (0.52 eÅ^{-5}), to form extended chain-like C–H···H–C contacts along the b-axis in **2AP**. Derivatives **1**, **2'** and **2''AP** lack intermolecular C–H···H–C interaction as confirmed through QTAIM calculations.

Similar electronegativity differences between involved sp^3 C–H bonds could only arise from electrically neutral hydrogens in the vicinity. Influence of adjacent carbonyl group may impart repulsive C–H···H–C interactions from first order electrostatic contribution. C–H···H–C contacts could be due to second-order mutual polarization of distorted charge clouds of the C–H bonds due to vicinal carbonyl group. Carbonyl group adjacent to the interacting sp^3 methyl groups could make the C–H bonds both polarizable and polarizing with respect to each other, as observed for B–H bonds.[29] **3AP** exhibits (CH_3) H···H (aryl) interactions whereas **4AP** shows bond path for (CH_3) H···H (CH_3) and (CH_3) H···H (aryl) interactions (Fig. S2b-c, ESI†). QTAIM calculations also confirmed the existence of C–H···O and C–H···C interactions in the derivatives **2**–**4AP**, apart from the C–H···H–C contacts (Table S4, ESI†).

Hirshfeld surface analyses[30] of **1**–**4AP** (Fig. 1 and Table S5, ESI†) exhibit systematic trends in the weak interactions with increase in number of substituted acetyl groups per pyrene unit as the following i) decrease in the C···H contacts that corresponds to σ-π (edge-to-face) interactions; ii) increase in the C···C contacts that corresponds to π-π (face-to-face) interactions; iii) increase in the O···H contacts that corresponds to C–H···O interactions; iv) increase in the H···H contacts that corresponds to dihydrogen interactions and v) increase in the O···C contacts that corresponds to dipolar interactions between the carbonyl groups. Concurrence of such weak intermolecular interaction dictates the molecular packing that results

Table 1. Calculated topological properties of the electron density for the intermolecular interaction in **2**–**4AP**.

	C–H···H–C contacts	[a]*d*, (Å)	[b]$\rho_b(\mathbf{r})$, (eÅ^{-3})	[c]$\nabla^2\rho_b(\mathbf{r})$, (eÅ^{-5})	[d]DE, (kJmol^{-1})
2AP	H18c···H'18c	2.230	0.036	0.520	3.46
3AP	H20c···H'8	2.246	0.041	0.471	4.29
	H20c···H'9	2.579*	0.019	0.249	1.87
4AP	H'18c···H"22c	2.239	0.040	0.514	4.32
	H'4···H18a	2.394	0.034	0.450	3.50
	H'5···H18c	2.577*	0.023	0.300	2.29

[a]*d*=distance, [b]$\rho_b(r)$=electron density at the BCP, [c]$\nabla^2\rho_b(r)$=Laplacian of $\rho_b(r)$ and [d]DE=dissociation energy (see ESI† for details). *Though H···H distance is > 2.4 Å, QTAIM exhibited electron density at (3, –1) BCP.

in ideal columnar 2D stacks in **4AP** having ρ=0.46 (Fig. 2). A value of ρ=19.5 in **1AP** indicates the formation of herringbone structure in the crystalline lattice when compared to the sandwich herringbone structure in the **P** (ρ=3.4). Efficient reduction in the ρ value from **1**–**4AP** is a consequence of simultaneous i) decrease in the percentage of C···H contacts (σ-π stacking) from 46.9% (**1AP**) to 7.4% (**4AP**) and ii) increase in the C···C contacts (π-π stacking) from 2.4% (**1AP**) to 16.1% (**4AP**). With increase in the number of acetyl groups in the pyrene core, crystal packing of **1**–**4AP** shows distinct patterns through a gradual decrease in the interplanar angle between the adjacent pyrene units (θ=48.4° for **1AP** and θ=0° for **4AP**; Fig. S3 and Table S6, ESI†). Decrease in the interplanar angle accompanies with the transformation of herringbone structure of **1AP** to columnar structure of **4AP**. **2'AP** shows herringbone packing without π-π overlap between adjacent pyrene units while crystal structure of **2**, **2"AP** show a lamellar motif with 2D π-π stacking (brickwork/γ-motif). Torsional angle between the planes of adjacent pyrene units in **2**, **2"AP** is found to be 0° and 1° respectively (Fig. S4-S5, ESI†). **3AP** shows columnar stacks with extended 2D π-π stacking (β-motif), consistent with **4AP**. While **3AP** exhibited a torsional angle of 67.8° between the planes of adjacent pyrene units, near-orthogonal (80.4°) arrangement of pyrene units was observed for **4AP**, consistent with the 1,3,6,8-tetraphenylpyrene derivatives reported by Geerts, Bredas and coworkers.[31] We observed π-π stacking distance of 3.4-3.5 Å in **4AP** when compared to 4.8 Å in 1,3,6,8-tetrakis(4-methoxyphenyl)-pyrene reported earlier.[31] By virtue of the smaller size of the acetyl *vs*. phenyl substituents, we observed shorter π-π stacking distance in **4AP**.

In **2AP**, carbonyl oxygen interacts with the aryl hydrogen (C–H···O; Fig. S6, ESI†) forming a zig-zag arrangement along b-axis (out-of-plane; 1D), while **2'AP** favors linear arrangement along c-axis possessing C–H···O interactions. Interplanar angle of 14.5° between the pyrene units in **2"AP** arises from C–H···O contacts. Extended C–H···O interactions in **3**–**4AP** across the ab-plane promote sheet-like arrangement of pyrene units (Fig. S6, ESI†) in combination with interplanar C–H···O interactions that support the pyrene (β-structure) stacks along the c-axis. In addition to C–H···O interactions, we observed C–H···H–C contacts (3.46 - 4.32 kJ mol^{-1}; Table 1) in crystalline **2**–**4AP**. C–H···H–C contacts in **2AP** (b-axis; in-plane; 1D) and **3AP** (a-axis; in-plane; 1D) promote the linear arrangement of the pyrene units. In **4AP**, C–H···O interactions promote stacks along c-axis that is reinforced by C–H···H–C contacts across the ab-plane.

We performed steady-state and time-resolved photophysical measurements to correlate the extent of overlap between adjacent pyrene units *vs*. colour properties in crystalline **1**–**4AP**. Experiments were also carried out in dilute solutions of chloroform to understand the photophysical properties of **1**–**4AP**. Increasing number of acetyl groups resulted in progressive red-shift in the UV- Vis absorption

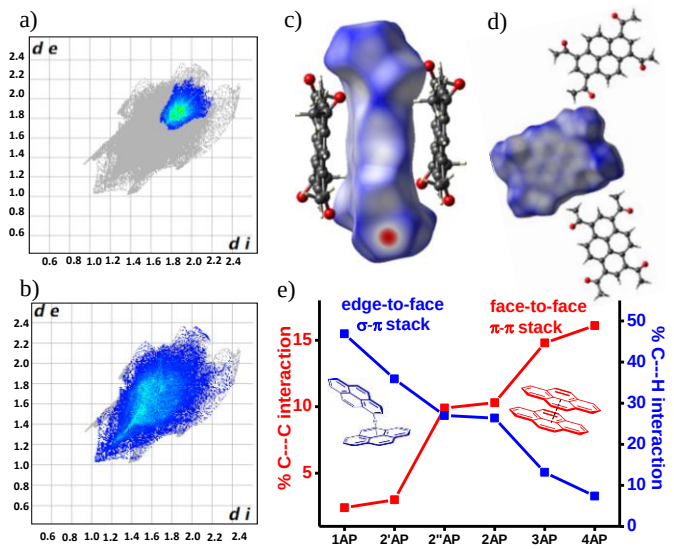

Fig. 1 Hirshfeld 2D fingerprint plot of **4AP** with the region of the plots corresponding to a) C⋯C and b) H⋯H interactions; Hirshfeld surface of **4AP** mapped with d_{norm} depicting c) C⋯C and d) H⋯H interactions; e) percentage contribution of edge-to-face (C⋯H) and face-to-face (C⋯C) interactions in **1**–**4AP**.

maximum of **1**–**4AP** in chloroform, for example 22 nm (**1AP**) and 70 nm (**4AP**), when compared to the **P** (Table S7, Fig. S7a, ESI†). Upon excitation at 350 nm, emission maximum of **1**–**4AP** in chloroform exhibited similar trend indicating the role of extended conjugation arising from carbonyl group(s) in the electronic transitions in pyrene unit (Fig. S7b, ESI†). We observed a significant decrease in the fluorescence quantum yield of **1**–**4AP** (Φ_f < 0.9%, Table S7, ESI†) in chloroform when compared to **P** (Φ_f = 75%).[32] Observed low Φ_f of **1**–**4AP** in chloroform could be attributed to alternate excited state decay pathways ($k_{nr} \approx k_{ISC} >>> k_r$) due to the incorporation of acetyl group(s).[16] Picosecond time-resolved fluorescence measurements of **1**–**4AP** in chloroform exhibits short lifetime (τ_f = 1-2 ns) when monitored at respective emission maximum upon excitation at 375 nm (Fig. S8, ESI†). While **2**–**4AP** in chloroform shows longer lifetime (ca. 3-5 ns) when monitored at longer wavelength (500-550 nm) indicating the possibility of aggregation. Emission wavelength dependent excitation (Fig. S9, ESI†) in combination with concentration dependent emission (Fig. S10, ESI†) and excitation (Fig. S11, ESI†) spectra confirms the existence of ground state aggregate in **2-4AP** in $CHCl_3$.

In the crystalline state, **1**–**4AP** exhibited diverse colour ranging (Scheme 1, Row III) from pale yellow-yellow-orange resulting in a red-shift of 100 nm in the absorption maximum of **4AP** when compared to **P** (Fig. S12, ESI†). Upon excitation at 350 nm, **1**–**4AP** exhibited a remarkable red-shift, for example 174 nm in the case of **4AP**, in the emission maximum when compared to **P** (Scheme 1, Row IV and Figs. S12b-S13, ESI†).[32] Red-shift in the excimer-like fluorescence of **1**–**4AP** could be attributed to a combination of additional conjugation from acetyl groups and increase in the extent of overlap between the adjacent pyrene moieties.[7] A significant red-shift in the excitation spectra of **1**–**4AP** when compared to the corresponding absorption spectra is indicative of ground state interaction between the vicinal pyrene units (Fig. S14, ESI†). Slip-stacked arrangement between the adjacent pyrene units in the crystalline **2**, **2'** and **2''AP** in combination with enhanced Φ_f, τ_f and k_r when compared to that in solution indicate the possibility of J-like aggregate and/or excimer of pyrene (Table S7, ESI†).[33] Aggregate induced enhanced emission (AIE) due to restricted motion of the

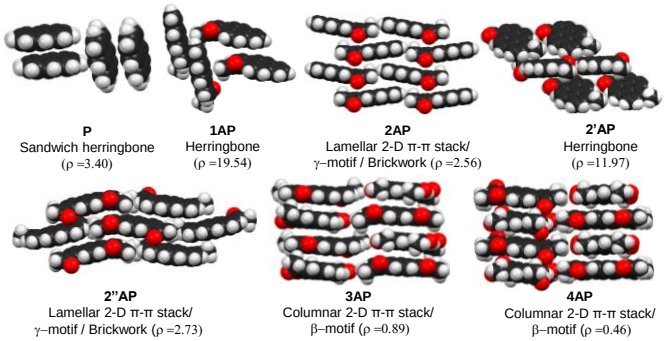

Fig. 2 Close packing arrangement in **1**–**4AP** indicating the values of ρ[(%C⋯H)/(%C⋯C)].[34] Herringbone (ρ>4.5), sandwich herringbone (3.2<ρ<4.0), γ (1.2<ρ<2.7), β (0.46<ρ<1.0).

flanking acetyl groups could also result in the enhanced fluorescence in the crystalline **2**, **2'** and **2''AP**.[35] Enhanced Φ_f in **3**–**4AP** could be attributed to a combination of AIE, ground state aggregation and cross-dipole arrangement of the adjacent pyrene moieties as reported earlier.[31, 36] Among all the crystalline derivatives **1**–**4AP**, non-linear increase in the emission maximum of **3**–**4AP** could be a consequence of orbital overlap between the adjacent pyrene units from near-orthogonal arrangement.

In summary, we modulated the extent of π-π overlap between vicinal pyrene units through successive acylation. Unprecedented heteropolar dihydrogen contacts (sp^2 C–H⋯H–C sp^3) in organic crystals are established using QTAIM. Hirshfeld surface analysis is indicative of increase in π-π interactions and a concomitant decrease in the σ-π interactions with increase in number of acetyl groups per pyrene unit. A combination of C–H⋯H–C, C–H⋯O and π-π interactions facilitate the transformation of sandwich herringbone packing of **P** to herringbone arrangement in **1** and **2'AP**, brickwork arrangement in **2** and **2''AP** and columnar stacks in **3**–**4AP**. A systematic decrease in the interplanar angle between the vicinal pyrene units could be attributed to the dramatic shift in the emission spectra (ca. 42–174 nm) of crystalline **1**–**4AP** when compared to pyrene. J-like aggregation and/or AIE in the crystal packing of **1**–**4AP** corroborates to moderately emissive blue-green-orange crystals. Efforts are progressing in our laboratory to correlate the photoconduction *vs.* crystal packing of acetylpyrene derivatives.

Acknowledgements

Authors dedicate this work to Professor M. V. George on the occasion of his 86th birthday. M. H. acknowledges the Science and Engineering Research Board (SERB) for the support of this work, SERB/F/0962. Authors thank Mr. Alex P. Andrews for X-ray crystal structure analysis of **1**–**4AP**. S. K. R. and K. N. acknowledge Council of Scientific and Industrial Research, India for the Research Fellowship. The authors gratefully acknowledge the anonymous Reviewers for their valuable comments and suggestions to improve the quality of the manuscript.

Notes and references

*School of Chemistry, Indian Institute of Science Education and Research Thiruvananthapuram, CET Campus, Sreekaryam, Thiruvananthapuram, Kerala, INDIA 695016. E-mail: mahesh@iisertvm.ac.in

†Electronic Supplementary Information (ESI) available: Experimental details, summary of crystal structure and refinement details of **1**–**4AP**. CCDC 984436-984441. See DOI: 10.1039/c000000x/

1. M. D. Hollingsworth, *Science*, 2002, **295**, 2410-2413.

2. (a) J. D. Servaites, B. M. Savoie, J. B. Brink, T. J. Marks and M. A. Ratner, *Energy Environ. Sci.*, 2012, **5**, 8343-8350; (b) G. Raffy, D. Ray, C.-C. Chu, A. Del Guerzo and D. M. Bassani, *Angew. Chem., Int. Ed.*, 2011, **50**, 9584-9588; (c) B. Kahr, J. Freudenthal and E. Gunn, *Acc. Chem. Res.*, 2010, **43**, 684-692.
3. (a) D. J. Lipomi and Z. Bao, *Energy Environ. Sci.*, 2011, **4**, 3314-3328; (b) S. Varughese, *J. Mater. Chem. C*, 2014, **2**, 3499-3516; (c) J. E. Anthony, *Chem. Rev.*, 2006, **106**, 5028-5048; (d) T. Kawai, Y. Nakashima and M. Irie, *Adv. Mater.*, 2005, **17**, 309-314.
4. (a) B. Kippelen and J.-L. Bredas, *Energy Environ. Sci.*, 2009, **2**, 251-261; (b) G. R. Hutchison, M. A. Ratner and T. J. Marks, *J. Am. Chem. Soc.*, 2005, **127**, 16866-16881; (c) H. Moon, R. Zeis, E.-J. Borkent, C. Besnard, A. J. Lovinger, T. Siegrist, C. Kloc and Z. Bao, *J. Am. Chem. Soc.*, 2004, **126**, 15322-15323.
5. J. E. Anthony, J. S. Brooks, D. L. Eaton and S. R. Parkin, *J. Am. Chem. Soc.*, 2001, **123**, 9482-9483.
6. (a) Q. Feng, M. Wang, B. Dong, C. Xu, J. Zhao and H. Zhang, *CrystEngComm*, 2013, **15**, 3623-3629; (b) Y.-C. Chang, Y.-D. Chen, C.-H. Chen, Y.-S. Wen, J. T. Lin, H.-Y. Chen, M.-Y. Kuo and I. Chao, *J. Org. Chem.*, 2008, **73**, 4608-4614.
7. Q. Feng, M. Wang, B. Dong, J. He and C. Xu, *Cryst. Growth Des.*, 2013, **13**, 4418-4427.
8. T. Mutai, H. Satou and K. Araki, *Nat. Mater.*, 2005, **4**, 685-687.
9. (a) K. Nagura, S. Saito, H. Yusa, H. Yamawaki, H. Fujihisa, H. Sato, Y. Shimoikeda and S. Yamaguchi, *J. Am. Chem. Soc.*, 2013, **135**, 10322-10325; (b) X. Sun, X. Zhang, X. Li, S. Liu and G. Zhang, *J. Mater. Chem.*, 2012, **22**, 17332-17339.
10. H. Ito, M. Muromoto, S. Kurenuma, S. Ishizaka, N. Kitamura, H. Sato and T. Seki, *Nat. Commun.*, 2013, **4**.
11. S. Varghese and S. Das, *J. Phys. Chem. Lett.*, 2011, **2**, 863-873.
12. J. R. Lakowicz, in *3rd ed.*, Springer, New York, 2006.
13. (a) R. T. Cheriya, K. Nagarajan and M. Hariharan, *J. Phys. Chem. C*, 2013, **117**, 3240-3248; (b) R. T. Cheriya, J. Joy, A. P. Alex, A. Shaji and M. Hariharan, *J. Phys. Chem. C*, 2012, **116**, 12489-12498.
14. R. T. Cheriya, A. R. Mallia and M. Hariharan, *Energy Environ. Sci.*, 2014, **7**, 1661-1669.
15. C. Friedel and J. M. Crafts, *J. Chem. Soc.*, 1877, **32**, 725-791.
16. Y. Niko, Y. Hiroshige, S. Kawauchi and G. Konishi, *J. Org. Chem.*, 2012, **77**, 3986-3996.
17. F. D. Lewis and J.-S. Yang, *J. Phys. Chem. B*, 1997, **101**, 1775-1781.
18. T. Hassheider, S. A. Benning, H.-S. Kitzerow, M.-F. Achard and H. Bock, *Angew. Chem., Int. Ed.*, 2001, **40**, 2060-2063.
19. (a) T. M. Figueira-Duarte and K. Müllen, *Chem. Rev.*, 2011, **111**, 7260-7314; (b) A. Hayer, V. de Halleux, A. Köhler, A. El-Garoughy, E. W. Meijer, J. Barberá, J. Tant, J. Levin, M. Lehmann, J. Gierschner, J. Cornil and Y. H. Geerts, *J. Phys. Chem. B*, 2006, **110**, 7653-7659.
20. G. R. Desiraju, *Acc. Chem. Res.*, 1996, **29**, 441-449.
21. S. Paliwal, S. Geib and C. S. Wilcox, *J. Am. Chem. Soc.*, 1994, **116**, 4497-4498.
22. J. Echeverria, G. Aullon, D. Danovich, S. Shaik and S. Alvarez, *Nature Chem.*, 2011, **3**, 323-330.
23. E. V. Anslyn and D. A. Dougherty, *Modern Physical Organic Chemistry*, University Science Books, Sausalito, CA, 2006.
24. H. Vollmann, H. Becker, M. Corell and H. Streeck, *Justus Liebigs Ann. Chem.*, 1937, **531**, 1-159.
25. J. B. Birks, A. A. Kazzaz and T. A. King, *Proc. R. Soc. A*, 1966, **291**, 556-569.
26. A. Camerman and J. Trotter, *Acta Crystallogr.*, 1965, **18**, 636-643.
27. V. I. Bakhmutov, *Dihydrogen Bond: Principles, Experiments, and Applications*, John Wiley & Sons, Inc., Hoboken, New Jersey, 2008.
28. (a) R. F. W. Bader, *Atoms in Molecules: A Quantum Theory*, Oxford University Press, Oxford, U.K., 1990; (b) A. Volkov, P. Macchi, L. J. Farrugia, C. Gatti, P. R. Mallinson, T. Richter and T. Koritsanszky, User Manual, 2006 edn., vol. XD2006, a computer program package for multipole refinement, topological analysis of charge densities and evaluation of intermolecular energies from experimental or theoretical structure factors, pp. User Manual, 2006.
29. D. J. Wolstenholme, J. Flogeras, F. N. Che, A. Decken and G. S. McGrady, *J. Am. Chem. Soc.*, 2013, **135**, 2439-2442.
30. S. K. Wolff, D. J. Grinwood, J. J. McKinnon, M. J. Turner, D. Jayatilaka and M. A. Spackman, University of Western Australia, Perth, Australia, 2012.
31. V. de Halleux, J. P. Calbert, P. Brocorens, J. Cornil, J. P. Declercq, J. L. Brédas and Y. Geerts, *Adv. Funct. Mater.*, 2004, **14**, 649-659.
32. R. Katoh, K. Suzuki, A. Furube, M. Kotani and K. Tokumaru, *J. Phys. Chem. C*, 2009, **113**, 2961-2965.
33. (a) F. C. Spano, *Acc. Chem. Res.*, 2009, **43**, 429-439; (b) J. Gierschner, L. Lüer, B. Milián-Medina, D. Oelkrug and H.-J. Egelhaaf, *J. Phys. Chem. Lett.*, 2013, **4**, 2686-2697; (c) U. Rösch, S. Yao, R. Wortmann and F. Würthner, *Angew. Chem., Int. Ed.*, 2006, **45**, 7026-7030.
34. L. Loots and L. J. Barbour, *CrystEngComm*, 2012, **14**, 300-304.
35. (a) Y. Hong, J. W. Y. Lam and B. Z. Tang, *Chem. Soc. Rev.*, 2011, **40**, 5361-5388; (b) S.-L. Tou, G.-J. Huang, P.-C. Chen, H.-T. Chang, J.-Y. Tsai and J.-S. Yang, *Chem. Commun.*, 2014, **50**, 620-622.
36. (a) M. Shimizu and T. Hiyama, *Chem. Asian J.*, 2010, **5**, 1516-1531; (b) Z. Xie, B. Yang, F. Li, G. Cheng, L. Liu, G. Yang, H. Xu, L. Ye, M. Hanif, S. Liu, D. Ma and Y. Ma, *J. Am. Chem. Soc.*, 2005, **127**, 14152-14153.

Table of Contents: Graphical Abstract

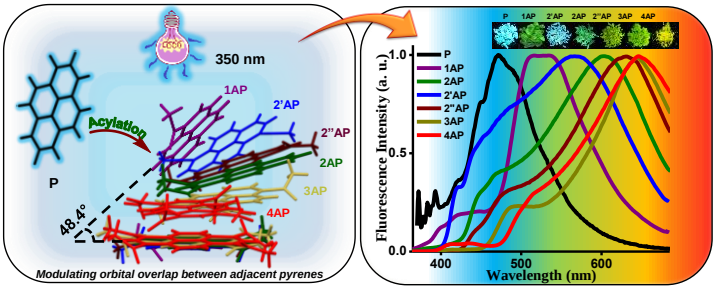

Sandwich herringbone-herringbone-brickwork-columnar crystal ordering, achieved through successive Friedel–Crafts acylation of pyrene, forms the basis for diverse solid-state colouring and blue-green-orange fluorescent crystals.